LANGMUIR Article
Cite This: Langmuir 2017, 33, 12434-12442 pubs.acs.org/Langmuir

Structural Characterization of Rh and RhAu Dendrimer-Encapsulated Nanoparticles

Long Luo,[†,∥] Janis Timoshenko,[§,∥] Aliya S. Lapp,[†] Anatoly I. Frenkel,[*,§] and Richard M. Crooks[*,†]

[†]Department of Chemistry and Texas Materials Institute, The University of Texas at Austin, 105 E. 24th Street, Stop A5300, Austin, Texas 78712, United States

[§]Department of Materials Science and Chemical Engineering, Stony Brook University, Stony Brook, New York 11794, United States

Supporting Information

ABSTRACT: We report the structural characterization of 1−2 nm Rh and RhAu alloy dendrimer-encapsulated nanoparticles (DENs) prepared by chemical reduction with $NaBH_4$. In contrast to previously reported results, in situ and ex situ X-ray absorption spectroscopic experiments indicate that only a fraction of the Rh^{3+} present in the precursors are reduced by $NaBH_4$. Additional structural analysis of RhAu alloy DENs using extended X-ray absorption fine structure spectroscopy leads to a model in which there is significant segregation of Rh and Au within the nanoparticles. In Rh-rich alloy DENs, Au atoms are segregated on the nanoparticle surface.

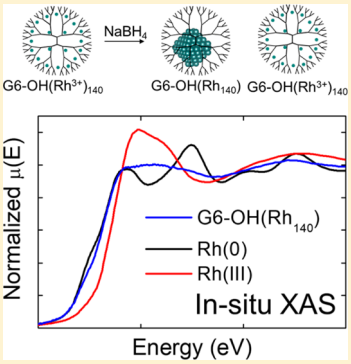

INTRODUCTION

Rh-containing monometallic and bimetallic nanoparticles (NPs) are active catalysts for the hydrogenation of olefins and aromatic compounds[1−4] and CO oxidation.[5−7] Even for these relatively simple reactions, however, it is challenging to obtain reliable mechanistic information because the NP catalysts are often structurally heterogeneous. Dendrimer-encapsulated nanoparticle (DENs) catalysts are well-suited for addressing this problem because they can be nearly monodisperse in size, composition, and structure.[8] DENs are typically synthesized by complexing metal ions with poly(amidoamine) (PAMAM) dendrimers and then reducing with $NaBH_4$. The size of DENs depends on the number of metal ions initially complexed within the dendrimer,[9] and once formed, DENs are retained and stabilized within the dendrimer interior.[9]

There are a few reports in the literature describing the synthesis of Rh DENs and RhM (M = Pd and Ru) alloy DENs and their use in catalysis.[10−15] However, there is no consensus regarding the actual structure of even monometallic Rh DENs. For example, Somorjai and co-workers prepared Rh DENs containing an average of 30 atoms within fourth-generation, hydroxyl-terminated PAMAM dendrimers (G4-OH) by reducing a precursor complex (G4-OH$(Rh^{3+})_{30}$) with $NaBH_4$. Microscopy indicated that the diameter of the resulting materials was ∼1.0 nm,[12] which is close to the theoretical size of NPs containing 30 Rh atoms: 0.7 nm. However, X-ray photoelectron spectroscopy (XPS) showed that only about half of the Rh atoms in these G4-OH(Rh_{30}) DENs were metallic whereas the remaining fraction was oxidized. They proposed two possible explanations for this significant degree of oxidation: (1) postsynthesis oxidization of G4-OH(Rh_{30}) by air during the preparation of the XPS samples and (2) incomplete reduction of the G4-OH$(Rh^{3+})_{30}$ DEN precursor during synthesis. In a follow-up article,[13] the same group reported that the initial reduction of G4-OH(Rh^{3+}) was complete, which ruled out the second possibility.

In contrast to the results of Somorjai, Amiridis and co-workers reported a completely different structure for Rh DENs, synthesized using the same basic approach, using in situ extended X-ray absorption fine structure (EXAFS) spectroscopy.[16] They concluded that isolated Rh clusters, containing an average of 3 atoms, formed during the synthesis of DENs because the average Rh−Rh coordination number (CN) was as small as 2.2.

Here, we revisit this debate and reconcile the previous reports using both in situ and ex situ EXAFS and other analytical methods. The key finding is that only ∼60% of the G4-OH(Rh^{3+}) DEN precursor is reduced by $NaBH_4$ to metallic Rh. A similar structural analysis was carried out for RhAu alloy DENs, and the result was similar: incomplete reduction of the Rh fraction of the alloy. More interestingly, significant segregation of Rh and Au was observed in these RhAu DENs. Specifically, Au atoms tend to reside on the surface of Rh-rich RhAu DENs (those having atomic Rh/Au ratios >1), whereas this trend is reversed for Au-rich RhAu DENs. These structural results will be important for relating structure to function in future catalysis studies.

Received: August 13, 2017
Revised: September 21, 2017
Published: October 9, 2017

DOI: 10.1021/acs.langmuir.7b02857
Langmuir 2017, 33, 12434−12442

EXPERIMENTAL SECTION

Chemicals. G6-OH dendrimers in methanol were purchased from Dendritech, Inc. (Midland, MI). The methanol was removed under vacuum, and deionized (DI) water was added to yield a solution concentration of 200.0 μM. The following chemicals were used as received without further purification: $RhCl_3{\cdot}xH_2O$, $HAuCl_4{\cdot}3H_2O$, and $NaBH_4$ (Sigma-Aldrich). Solutions were prepared using DI water from a Millipore Milli-Q water system (18.2 MΩ·cm).

DEN Synthesis. Rh DENs were prepared by adding 140 equiv of $RhCl_3{\cdot}xH_2O$ to a 10.0 μM aqueous G6-OH solution. Rh^{3+} was allowed to complex with the dendrimers overnight, and then a 10-fold excess of $NaBH_4$ in DI water was added to reduce the G6-OH$(Rh^{3+})_{140}$ complexes to G6-OH(Rh_{140}) DENs. Note that the subscripts for both the complexes and the DENs are intended only to represent the Rh/G6-OH ratio and are not meant to imply that all complexes or DENs contain exactly 140 Rh ions or atoms, respectively. However, we have previously shown that DENs can be remarkably monodisperse and that the initial metal ion-to-dendrimer ratio is often a good indicator of DEN size.[8,9]

For RhAu DENs, a similar procedure was followed. A predetermined number of equiv, n, of $RhCl_3{\cdot}xH_2O$ (n = 110, 70, and 30) were mixed with 10.0 μM aqueous solutions of G6-OH and allowed to complex overnight. Next, 140 − n equiv of $HAuCl_4$ were added to the G6-OH(Rh^{3+}) complexes. Within 2 min, a 10-fold excess of $NaBH_4$ was added to reduce the complexes to G6-OH(Rh_nAu_{140-n}) DENs.

Characterization. UV−vis absorbance spectra were obtained using a Hewlett-Packard HP8453 spectrometer and a 1.0 mm path length quartz cuvette. A 10.0 μM G6-OH solution in water was used for background correction.

TEM images of the DENs were obtained using a JEOL 2010F TEM. The samples were prepared by dropping ∼1 μL of freshly prepared DEN solution onto carbon-coated Cu TEM grids (400 mesh, Electron Microscopy Sciences) and then drying under a N_2 stream for <1 min.

XPS data were collected using a Kratos Axis Ultra spectrometer having a monochromatic Al Kα X-ray source. The Rh and RhAu DEN samples were prepared by drop casting 10.0 μL of a DEN ink (vide infra) onto an ∼1 cm^2 glassy carbon chip and drying under a N_2 stream. Data were analyzed using CasaXPS (Casa Software Ltd.).

EXAFS data were collected on beamline BL 2−2 at the Stanford Synchrotron Radiation Lightsource (SSRL) at Stanford University. Rh K-edge (23220 eV) and Au L_3-edge (11919 eV) X-ray absorption spectroscopy (XAS) data for Rh and RhAu DENs were acquired in transmission mode for ex-situ samples and in fluorescence mode for in situ samples.

For ex situ EXAFS characterization, dry DEN samples were prepared by mixing Vulcan EC-72R carbon (1.0 mg per 1.0 mL of DEN solution) with 100 mL of 10.0 μM freshly prepared Rh or RhAu DEN solutions. This yielded a DEN ink that was then lyophilized using a Labconco FreeZone 12 lyophilizer. The dry samples were packed into N_2-filled glass vials in a N_2 glovebox and stored in the same vial until used for XAS measurements. The DEN samples were mixed with BN and pressed into 13-mm-diameter pellets prior to the measurements.

For measurements at the Au L_3-edge, 15-cm-long ion chambers filled with gases were used as incident (I_0, N_2) and transmitted (I_1, Ar) beam detectors. Beam slit sizes were 0.5 mm (vertical) × 6 mm (horizontal), and the Si(220) double-crystal monochromator was detuned by 20%. For measurements at the Rh K-edge, the I_1 detector was a 30-cm-long ion chamber filled with a 1:1 Ar/Kr mixture. The I_0 detector was filled with Ar only, the vertical slit size was reduced to 0.1 mm, and the Si(220) monochromator was detuned by 10%.

For in situ experiments, a 100 μM solution of Rh DENs was freshly prepared just prior to analysis at the beamline by reducing the G6-OH(Rh^{3+}) complexes in an ∼1-cm-thick solution cell having Kapton tape windows. Photographs of the solution cell are provided in Figure S1. Oxidation of the sample was avoided by flowing H_2 slightly above the solution during the entire in situ experiment. At both the Rh K-edge and the Au L_3-edge, the I_0 detector was filled with a 3:1 mixture of N_2 and Ar. Detuning of the Si(220) double-crystal monochromator by 20% was applied, and the slit sizes were 0.15 mm × 3.5 mm. A passivated, implanted planar silicon detector was used as the fluorescence detector. At least two energy scans were acquired and averaged for each sample to improve the signal-to-noise ratio. Rh and Au foil reference spectra were collected concurrently with the DEN spectra for energy calibration and data alignment and to obtain the amplitude reduction factors (S_0^2). XAS data were processed using the Athena software package.[17,18]

RESULTS AND DISCUSSION

Rh DEN Synthesis and UV−Vis Analysis. Details of the synthesis of G6-OH(Rh_{140}) DENs are provided in the Experimental Section but are also briefly summarized here. In the first step of the synthesis, 140 equiv of Rh^{3+} is mixed with the G6-OH dendrimer for ∼16 h. This results in the formation of a G6-OH$(Rh^{3+})_{140}$ precursor complex. The presence of this complex is apparent because the solution color changes from light brown to pale yellow (Figure 1a). The UV−vis spectra in

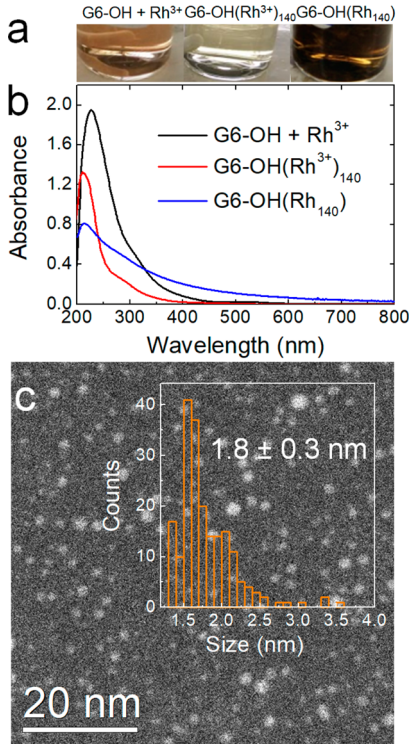

Figure 1. (a) From left to right, photographs of the initial mixture of the G6-OH dendrimer and $RhCl_3$ in a molar ratio of 1:140 (G6-OH + Rh^{3+}), the Rh-dendrimer complex (G6-OH$(Rh^{3+})_{140}$), and Rh DENs synthesized by the reduction of the precursor with $NaBH_4$ (G6-OH(Rh_{140})). (b) UV−vis spectra of the materials indicated in the legend. The data were acquired using a 1.0 mm quartz cuvette and blanked with a 10.0 μM G6-OH solution. (c) STEM image and size distribution histogram for G6-OH(Rh_{140}) DENs.

Figure 1b, which correspond to the first two photographs in Figure 1a (black and red lines, respectively), show that the absorption bands for the mixture of $RhCl_3$ and G6-OH at 228 and 314 nm decrease after 16 h. This change is probably a result of ligand exchange reactions involving chloride, the internal tertiary amines of G6-OH, and H_2O.[12] The new strong peak at ∼210 nm (red line) results from a ligand-to-metal

DOI: 10.1021/acs.langmuir.7b02857
Langmuir 2017, 33, 12434−12442

charge transfer associated with the formation of the metal ion/dendrimer complex.[19,20]

In the second step of the synthesis, a 10-fold excess of $NaBH_4$ is added to the precursor complex, and this results in the reduction of G6-OH$(Rh^{3+})_{140}$ to G6-OH(Rh_{140}) DENs. Evidence for this comes from the immediate change in solution color to dark brown (Figure 1a). Additionally, the UV−vis spectrum of the product G6-OH(Rh_{140}) DENs (blue line, Figure 1b) exhibits the expected broad-band absorption between 200 and 600 nm, corresponding to the formation of 1−2 nm NPs.[8,20−22] These changes in the UV−vis spectra during the Rh DEN synthesis are similar to those previously reported by Somorjai and co-workers.[12,13]

TEM and XPS Analysis of Rh DENs. To obtain direct evidence for Rh NP formation, we carried out TEM analysis of the G6-OH(Rh_{140}) DENs. The analysis of >100 randomly selected G6-OH(Rh_{140}) DENs (Figure 1c) indicates an average particle size of 1.8 ± 0.3 nm. This is close to the theoretical diameter (1.6 nm) for an M_{140} (M = Pt, Au, Pd, or Rh) NP having a truncated octahedral shape.[23−25]

Figure 2 is a high-resolution XPS spectrum of the G6-OH(Rh_{140}) DENs in the Rh 3d region. After fitting, two pairs

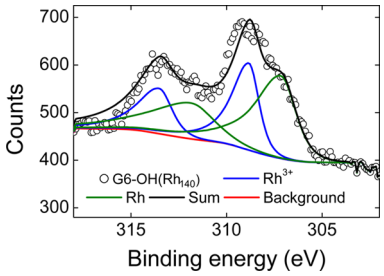

Figure 2. High-resolution XPS spectrum of G6-OH(Rh_{140}) DENs in the Rh 3d region.

of peaks are apparent. The Rh $3d_{5/2}$ peaks at 307.2 and 308.9 eV correspond to metallic and oxidized Rh, respectively, and on the basis of the peak areas, the percentages of each are 59 and 41%, respectively. Both the peak positions and extent of Rh^{3+} reduction for the G6-OH(Rh_{140}) DENs are close to the values for the much smaller G4-OH(Rh_{30}) DENs reported by the Somorjai group (Rh $3d_{5/2}$ peak positions, 307.3 and 309.2 eV; percentage of reduction, 56%).[12]

Somorjai and co-workers proposed two possible explanations for the oxidized Rh component in Rh DENs: (1) Rh oxidation by air during XPS sample preparation and (2) incomplete reduction of the G6-OH$(Rh^{3+})_{30}$ precursors.[12] In a follow-up study, the same group claimed that the reduction of G6-OH$(Rh^{3+})_{30}$ precursors was complete, suggesting that air exposure was responsible for the oxidized Rh signal in the XPS spectrum.[13] We believe, however, that the G6-OH-$(Rh^{3+})_{140}$ precursor is only partially reduced to Rh DENs by $NaBH_4$ during the synthesis. This hypothesis is inspired by the finding that the incomplete reduction of metal ion/G6-OH complexes has previously been observed for Pt DENs synthesized using the same method employed by Somorjai and us.[20,26]

For Pt DENs, we proposed that the distribution of reduced and oxidized Pt was bimodal, consisting of a fraction of fully reduced DENs and a fraction of a fully unreduced precursor complex. This conclusion relied, in part, on an early TEM study showing that Pt DENs had the correct size even though XPS revealed partial oxidation. We reasoned that if all of the DENs were only partially reduced then their size would be smaller.[26] Subsequently, we used high-resolution aberration-corrected STEM, which made it possible to distinguish between Pt atoms and ions and hence between the G6-OH$(Pt^{2+})_n$ precursors and G6-OH(Pt_n) DENs.[20] These STEM results, along with XAS, confirmed the bimodal distribution model for the incomplete reduction of the G6-OH$(Pt^{2+})_{140}$ precursor.

As discussed earlier, the G6-OH(Rh_{140}) DENs discussed here also have sizes close to the value expected for fully reduced G6-OH$(Rh^{3+})_{140}$ precursors, and XPS reveals that the precursor is only partially reduced. By analogy to the Pt DENs, therefore, we hypothesize a bimodal distribution of unreduced G6-OH$(Rh^{3+})_{140}$ precursors and fully reduced G6-OH(Rh_{140}) DENs. As in the Pt study, high-resolution, aberration-corrected STEM would be a good method for testing this hypothesis. However, the low Z-contrast of Rh precludes the possibility of imaging individual Rh ions and atoms.

X-ray Absorption Near-Edge Structure (XANES) Analysis of Rh DENs. Because of the limitations of TEM and XPS in distinguishing between fully reduced Rh DENs and fully unreduced Rh DEN precursors present in a bimodal mixture, we turned to in situ and ex situ XAS.[27,28] For the in situ XAS experiments, precautions were taken to prevent air oxidation of the G6-OH(Rh_{140}) DENs during measurements. Specifically, the G6-OH$(Rh^{3+})_{140}$ precursor was reduced with $NaBH_4$ immediately prior to data collection. Additionally, H_2 flowed over the solution during spectral acquisition. Photographs of the XAS cell are provided in Figure S1.

Figure 3a shows that the white-line intensity and the position of the absorption edge for the G6-OH(Rh_{140}) DENs prepared in situ are intermediate between those for Rh foil and Rh_2O_3, indicating the presence of an oxidized component in the sample. Because this sample was not exposed to air during the

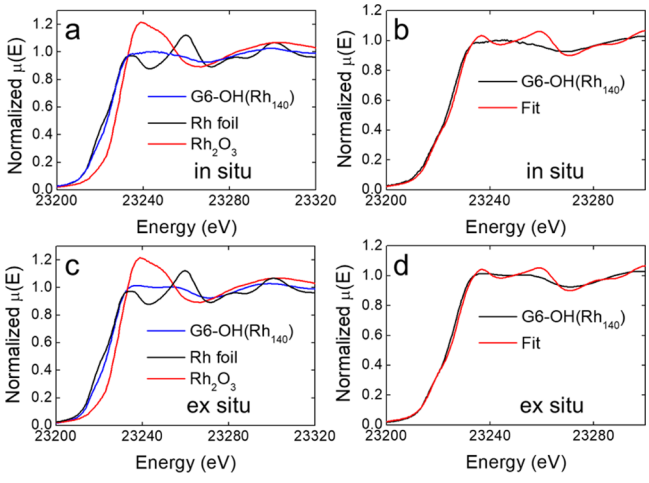

Figure 3. (a) XANES data and (b) LCA fit for a 50.0 μM G6-OH(Rh_{140}) solution prepared in situ. The G6-OH(Rh_{140}) solution was freshly synthesized in a homemade solution cell by adding a 10-fold excess of $NaBH_4$ to a 50.0 μM G6-OH$(Rh^{3+})_{140}$ solution. The G6-OH(Rh_{140}) solution was always under H_2 protection during XANES measurements. (c) XANES data and (d) LCA fit for a solid G6-OH(Rh_{140}) sample supported on Vulcan carbon (0.14 g of metal per 1 g of carbon) prepared ex situ. For both samples, XANES data for Rh foil and Rh_2O_3 were used as references for the LCA.

DOI: 10.1021/acs.langmuir.7b02857
Langmuir 2017, 33, 12434−12442

experiment, it is reasonable to believe that the G6-OH$(Rh^{3+})_{140}$ precursor was not fully reduced by $NaBH_4$.

XANES linear combination analysis (LCA) was used to quantify the extent of Rh reduction for comparison to the XPS results.[29] Figure 3b shows the spectrum of the in situ sample and the fit obtained from LCA using XANES spectra of Rh foil and Rh_2O_3 as references. The overlap between two curves is in reasonable agreement in that the shape and position of the absorption edge are accurately reproduced. The differences between the experimental XANES and LCA fits at higher energy are a consequence of the fact that XANES spectra for bulk materials (Rh foil and Rh_2O_3), which are used here as standards for the LCA fits, cannot describe perfectly the local structure of nanomaterials.[30−33] The important point is that LCA indicates that 69% of the Rh in the sample is in the reduced form, which compares favorably with the value of 59% determined by XPS (Table 1).

Table 1. Percentage Reduction of G6-OH$(Rh^{3+})_{140}$ DEN Precursors by $NaBH_4$ Reduction As Determined by the Indicated Methods

	percentage reduction		
	XPS	XANES, in situ	XANES, ex situ
G6-OH(Rh_{140})	59%	69%	65%

Figure 3c shows a XANES spectrum of a G6-OH(Rh_{140}) DEN sample prepared ex situ ~10 days before the XAS measurement. This sample was stored under N_2 from the time it was prepared until it was prepared for analysis. The corresponding LCA fit for this ex situ sample (Figure 3d) yields a nearly identical Rh reduction percentage (65%) as that of the in situ sample (69%). Because the ex situ DEN sample was exposed to air during the preparation of the sample pellet and throughout the ~1 h XAS measurement, we conclude that the oxidation of dry Rh DENs in air is a slow process.

Extended X-ray Absorption Fine Structure (EXAFS) Analysis of Rh DENs. As explained in the previous section, the DENs synthesized in situ and ex situ exhibit nearly the same percentage of reduction. This suggests that the G6-OH-$(Rh^{3+})_{140}$ precursor is only partially reduced by $NaBH_4$ and that the air oxidation of Rh DENs is a slow process. To better understand the structure of the Rh DENs, we now report on the results of a detailed EXAFS analysis of Rh DENs prepared both in situ and ex situ.

Nonlinear least-squares fitting to theoretical standards, as implemented in the FEFFIT code,[17] was utilized to analyze the EXAFS spectra of both Rh DEN samples.[27,34] Specifically, only nearest-neighbor contributions to the spectra were analyzed. The fitted variables were the coordination numbers (N), average interatomic distances (R), and bond-length disorder factors (σ^2) for both Rh−Rh and Rh−O pairs, which correspond to the reduced and unreduced G6-OH$(Rh^{3+})_{140}$ precursors, respectively. Note that unreduced Rh^{3+} is complexed with both the interior amines of G6-OH and water. In other words, there are both Rh−O and Rh−N bonds associated with the unreduced Rh^{3+}. Because EXAFS cannot distinguish between Rh−O and Rh−N contributions as a result of their similar photoelectron scattering properties, hereafter we use Rh−O to represent both contributions.

Correction to the photoelectron reference energy, ΔE_0, was fitted for each spectrum independently. Theoretical photoelectron scattering phases and amplitudes were obtained in self-consistent ab initio calculations using the FEFF8.5 code for bulk Rh and Rh_2O_3.[35] The complex exchange-correlation Hedin-Lundqvist potential and default values of muffin-tin radii, as provided within the FEFF8.5 code, were employed. Rh K-edge data fitting was carried out in the range from R_{min} = 1.0 Å up to R_{max} = 3.0 Å, and the Fourier transform was carried out in the k range from 2.5 to 12.0 $Å^{-1}$ (up to 9.0 $Å^{-1}$ for the in situ DEN sample). For the analysis of EXAFS data for Rh DENs, an amplitude reduction factor, S_0^2, of 0.8 was used. This value is intermediate between the S_0^2 values obtained for Rh foil (0.86) and Rh_2O_3 (0.73).

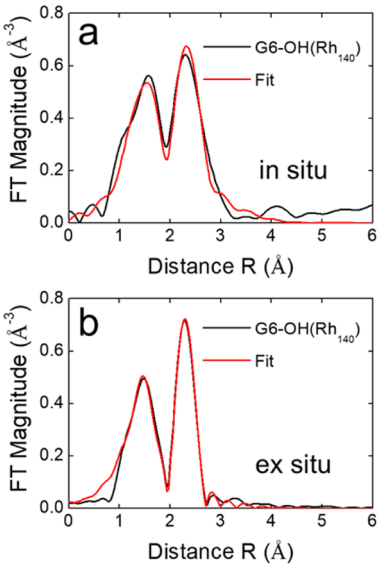

Figure 4. Magnitudes of k^2-weighted, Fourier-transformed Rh K-edge EXAFS data (black) and theoretical fits (red) for a 50.0 μM G6-OH(Rh_{140}) prepared in situ and for a G6-OH(Rh_{140}) solid sample supported on Vulcan carbon (ex situ). Both samples are the same as those used to acquire the data in Figure 3.

The fitting results are summarized in Figure 4 and Table 2. The fitting model yields reasonable agreement between experimental and theoretical EXAFS data, indicating that EXAFS supports the XANES data. That is, the concentration of Rh^{3+} is significant in both in situ and ex situ DEN samples. In other words, the putative G6-OH(Rh_{140}) DENs are likely composed of a mixture of two phases: reduced Rh in the NPs and unreduced Rh (present as Rh^{3+} ions complexed to the dendrimers or water). The extraction of coordination numbers from EXAFS spectra for such heterogeneous samples requires special care because they are averaged over all absorbing atoms in the sample. That is, if the sample is an inhomogeneous mixture, the coordination numbers for atoms in each of the nonequivalent environments are weighted by the molar fractions of each of the phases.[36] By definition, the apparent Rh−O coordination number (N_{Rh-O}) obtained from EXAFS analysis is given by eq 1.

$$N_{Rh-O} = \frac{n_{Rh-O}}{n_{Rh}} = \frac{x n_{Rh}}{n_{Rh}} \tilde{N}_{Rh-O} = x\tilde{N}_{Rh-O} \quad (1)$$

Here, n_{Rh} is the total number of Rh atoms in the sample, n_{Rh-O} is the total number of Rh−O bonds, x is the molar concentration of unreduced Rh^{3+} (which can be estimated from XANES LCA, Table 1), and $\tilde{N}_{Rh-O}$ is the actual average

DOI: 10.1021/acs.langmuir.7b02857
Langmuir 2017, 33, 12434−12442

Table 2. Structural Parameters Obtained by Fitting the Rh K-Edge EXAFS Data[a]

sample	N_{Rh-Rh}	N_{Rh-O}	R_{Rh-Rh}(Å)	R_{Rh-O} (A)	$\sigma_{Rh-Rh}{}^2(10^{-2}$ Å$^2)$	$\sigma_{Rh-O}{}^2(10^{-2}$ Å$^2)$	ΔE_0 (eV)
Rh_2O_3		6		2.02(2)		0.4(3)	−16(4)
G6-OH(Rh_{140}), in situ	3(1)	2(1)	2.70(2)	2.00(2)	0.3(4)	1(1)	−21(2)
G6-OH(Rh_{140}), ex situ	4.8(3)	2.4(3)	2.674(3)	2.023(5)	0.98(4)	0.8(1)	−21.5(4)
Rh foil	12		2.681(3)		0.40(3)		−19.0(7)

[a]The uncertainty of the last digit is given in parentheses.

number of oxygen atoms per Rh atom in unreduced Rh species (eq 2).

$$\tilde{N}_{Rh-O} = N_{Rh-O}/x \quad (2)$$

Similarly, because of the presence of unreduced Rh^{3+}, the actual coordination numbers for Rh−Rh bonds in the reduced phase ($\tilde{N}_{Rh-Rh}$) are equal to the apparent Rh−Rh coordination number (N_{Rh-Rh}, Table 2) multiplied by a factor of $1/(1-x)$.

The values of $\tilde{N}_{Rh-Rh}$ and $\tilde{N}_{Rh-O}$ for the Rh DENs are summarized in Table 3. The results indicate that the actual Rh−O coordination numbers ($\tilde{N}_{Rh-O}$) for the DENs prepared in situ and ex situ are close. Moreover, the Rh−O coordination numbers are consistent with expectations for bulk Rh_2O_3, and the Rh−Rh coordination number ($\tilde{N}_{Rh-Rh} \approx 7$) agrees reasonably well with that expected for NPs consisting of ∼140 atoms (9).[20] Note that $\tilde{N}_{Rh-Rh}$ for the in situ sample is significantly smaller than that for the ex situ sample. This is most likely an artifact of the analysis because only a very limited k range (from 2.5 to 9.0 Å^{-1}) was available for data fitting for this sample, and the coordination numbers correlate very strongly with disorder factors. As shown in Table 2, Rh−Rh and Rh−O bond distances for in situ and ex situ Rh DENs are close. The Rh−O distance is close to the corresponding distance in bulk Rh_2O_3, whereas the Rh−Rh distance is close to that for bulk Rh metal. These findings show that the local structures for ex situ and in situ samples are close and that in both cases there is a mixture of reduced Rh particles, having sizes of ∼1−2 nm, and unreduced Rh^{3+} species.

Table 3. Actual Rh−O and Rh−Rh Coordination Numbers ($\tilde{N}_{Rh-O}$ and $\tilde{N}_{Rh-Rh}$) after Correction for the Presence of the Reduced and Unreduced Phases[a]

	$\tilde{N}_{Rh-O}$	$\tilde{N}_{Rh-Rh}$
Rh_2O_3	6	
G6-OH(Rh_{140}), in situ	6(3)	4(1)
G6-OH(Rh_{140}), ex situ	7(1)	7(1)
Rh foil		12

[a]The uncertainty of the last digit is given in parentheses.

XANES and EXAFS Analyses of RhAu Bimetallic DENs. In addition to Rh-only DENs, we also prepared RhAu bimetallic alloy DENs having different percentage compositions. There have been a few previous studies of RhAu NPs.[1,37,38] For example, Humphrey and co-workers reported that RhAu bimetallic NPs, synthesized by a microwave-assisted method, exhibit improved activity for the hydrogenation of cyclohexene compared to monometallic Rh or Au NPs.[1] However, the origin of the activity improvement is not clear because these RhAu NPs were found to be structurally heterogeneous by TEM. By examining the structure of smaller, better-defined RhAu bimetallic DENs, we hoped to better understand the properties of these larger NPs.

As for the G6-OH(Rh_{140}) DENs, the XAS results for the G6-OH(Rh_xAu_{140-x}) (x = 30, 70, 110, and 140) DENs were qualitatively similar regardless of whether the reduction step was carried out in situ or ex situ. Therefore, we focus here on the analysis of the Rh K-edge and Au L_3-edge XAS data for just the RhAu DENs prepared ex situ. This is because the signal-to-noise ratio is significantly better than for the in situ DENs, making it possible to analyze the data over an extended range of wavenumbers, k.

XANES data for RhAu DEN samples prepared ex situ and analyzed at the Rh K-edge are shown in Figure S2. Regardless of composition, the white line intensities and the positions of the absorption edges for the RhAu DENs are intermediate

Table 4. Percentage of Reduced Rh in RhAu Alloy DENs ($1-x$) Obtained from XANES, Coordination Numbers (N) for Au−M and Rh−M Bonds in RhAu Alloy Samples (N_{Au-Au}, N_{Au-Rh}, $\tilde{N}_{Rh-Rh}$, and $\tilde{N}_{Rh-Au}$), Total Coordination Numbers for Au and Rh (N_{Au} and N_{Rh}), and Average Coordination Numbers (N_{metal}) in the Reduced Phase[a]

	$1-x$	$\frac{n_{Au}}{n_{Rh}(1-x)}$	N_{Au-Au}	N_{Au-Rh}	$\frac{N_{Au-Au}}{N_{Au-Rh}}$	conclusion
Au foil			12			
G6-OH($Rh_{30}Au_{110}$)	45%	8.1	8.5(5)	0.6(3)	14(7)	$\frac{N_{Au-Au}}{N_{Au-Rh}} > \frac{n_{Au}}{n_{Rh}(1-x)}$, bulk segregation
G6-OH($Rh_{70}Au_{70}$)	46%	2.2	7.0(5)	1.3(3)	5(1)	$\frac{N_{Au-Au}}{N_{Au-Rh}} > \frac{n_{Au}}{n_{Rh}(1-x)}$, bulk segregation
G6-OH($Rh_{110}Au_{30}$)	64%	0.43	5(1)	2.2(8)	2.3(9)	$\frac{N_{Au-Au}}{N_{Au-Rh}} > \frac{n_{Au}}{n_{Rh}(1-x)}$, bulk segregation
Rh foil			12			

	$\tilde{N}_{Rh-Au}$	$\tilde{N}_{Rh-Rh}$	N_{Rh}	N_{Au}	N_{metal}	conclusion
Au foil					12	
G6-OH($Rh_{30}Au_{110}$)	4(4)	0	4(4)	9.1(8)	9(1)	N/A
G6-OH($Rh_{70}Au_{70}$)	2(2)	7(7)	9(9)	8.3(8)	8(8)	N/A
G6-OH($Rh_{110}Au_{30}$)	3(1)	8(1)	11(2)	7(2)	10(4)	$N_{Au} < N_{Rh}$, Au-rich surface
Rh foil		12	12		12	

[a]The uncertainty of the last digit is given in parentheses.

DOI: 10.1021/acs.langmuir.7b02857
Langmuir 2017, 33, 12434−12442

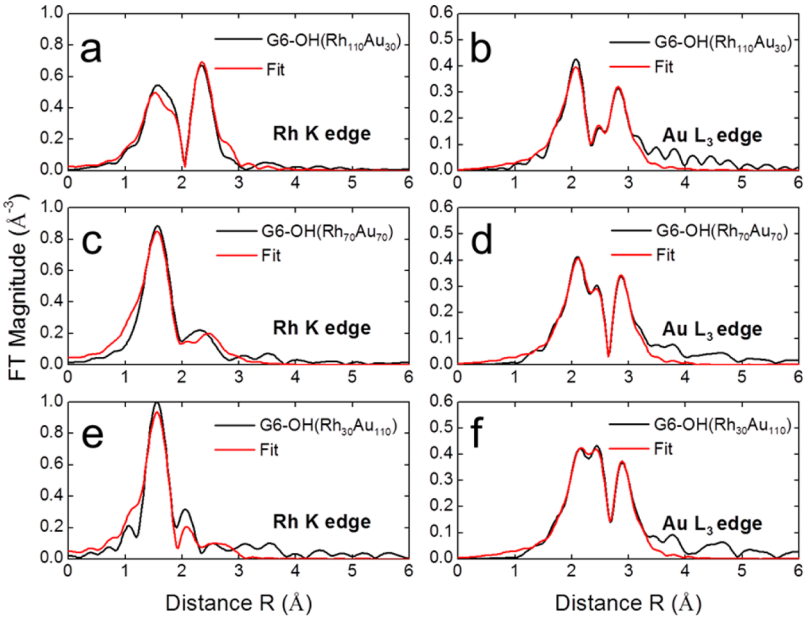

Figure 5. Magnitudes of k^2-weighted, Fourier-transformed Rh K-edge and Au L_3-edge EXAFS data (black) and theoretical fits (red) for the indicated RhAu bimetallic alloy DENs supported on Vulcan carbon (ex situ samples).

between those for Rh foil and Rh_2O_3. This suggests the coexistence of both reduced and unreduced Rh species as was observed for Rh-only DENs. The percentages of reduced Rh in the RhAu DENs were calculated by XANES LCA (Figure S3). The results in Table 4 show that only ~45 to 64% of the Rh^{3+} originally present in the precursors (G6-OH-$(Rh^{3+})_xAu^{3+}{}_{(140-x)}$) are reduced to metallic Rh by $NaBH_4$. In contrast, XANES data for the same DENs at the Au L_3-edge (Figure S4) indicate that the Au fraction of the precursors is fully reduced. From these observations, we conclude that the RhAu DENs consist of a mixture of reduced RhAu bimetallic NPs and unreduced Rh^{3+}.

EXAFS analysis was used to provide additional structural information about the RhAu DENs. In this case, the EXAFS data for both the Rh K-edge and Au L_3-edge were fitted simultaneously (Figure 5). In both cases, only contributions from the first coordination shell were analyzed because no significant contribution beyond the first two peaks of the Fourier transform was observed. The fitted variables were N, R, and σ^2 for the Rh−Rh, Rh−Au, Rh−O, Au−Au, and Au−Rh pairs. We constrained R and σ^2 for the Rh−Au and Au−Rh pairs to be equal, and corrections to the photoelectron reference energy, ΔE_0, were independently fitted for each Rh K-edge and Au L_3-edge spectrum. For the Au L_3-edge, data fitting was carried out in the range from R_{min} = 1.2 Å up to R_{max} = 3.4 Å, and the Fourier transform was carried out in the k range from 2.5 $Å^{-1}$ up to 14.0 $Å^{-1}$. The $S_0{}^2$ factor (0.95 ± 0.06) was obtained from the fitting of Au foil data. The Rh K-edge parameters used for fitting the Rh-only DENs were also used for the bimetallic DENs.

The results of the EXAFS analysis are summarized in Tables 4 and S1. Apparent Rh-M coordination numbers obtained from EXAFS data fitting (N_{Rh-Rh} and N_{Rh-Au}, Table S1) were corrected for the presence of unreduced Rh species using eq 2. The actual coordination numbers ($\tilde{N}_{Rh-Rh}$ and $\tilde{N}_{Rh-Au}$) in the reduced phase are listed in Table 4. The actual total coordination numbers for reduced Rh, N_{Rh}, can be calculated using eqs 3 and 4 for Rh and Au, respectively.

$$N_{Rh} = \tilde{N}_{Rh-Rh} + \tilde{N}_{Rh-Au} \quad (3)$$

$$N_{Au} = \tilde{N}_{Au-Rh} + \tilde{N}_{Au-Au} \quad (4)$$

The actual Au−Rh and Au−Au coordination numbers, N_{Au-Rh} and N_{Au-Au}, respectively, are equal to the apparent Au−Rh and Au−Au coordination numbers, $\tilde{N}_{Au-Rh}$ and $\tilde{N}_{Au-Au}$ (obtained from EXAFS fitting) because XANES spectra for the Au L_3-edge indicate no evidence of Au oxidation. The average coordination number in the reduced phase (N_{metal}), which includes both Au and Rh, is calculated from eq 5.[36]

$$N_{metal} = \frac{n_{Rh}(1-x)N_{Rh} + n_{Au}N_{Au}}{n_{Rh}(1-x) + n_{Au}} = \frac{(1-x)N_{Rh} + (n_{Au}/n_{Rh})N_{Au}}{(1-x) + n_{Au}/n_{Rh}} \quad (5)$$

Here, n_{Rh} and n_{Au} are the total numbers of Rh and Au atoms, respectively, in the sample, and $(1-x)n_{Rh}$ is the total number of Rh atoms in the reduced phase.

Using the data in Tables 4 and S1, it is possible to draw conclusions about the structures of the reduced RhAu DENs. This analysis is carried out as follows. First, we estimated the average size of the NPs using N_{metal}. As shown in Table 4, N_{metal} is close to 8−9 for all DENs, which corresponds to NPs having sizes of ~1−2 nm, which is in excellent agreement with the TEM results (1.8−2.2 nm, Figure S5). This level of agreement validates the EXAFS modeling procedure. It also confirms the XANES analysis of the fractions of Rh atoms in the reduced and unreduced states. Specifically, the high Rh−O coordination numbers together with the high values for N_{Rh}, derived from EXAFS fitting, indicate the coexistence of fully reduced metallic particles and unreduced Rh^{3+} species, as previously observed for pure Rh DENs.

Second, the degree of segregation of Au and Rh atoms in the DENs was evaluated by comparing the Au−Rh (N_{Au-Rh}) and Au−Au (N_{Au-Au}) coordination numbers in the reduced phase. For a random alloy, the ratio of N_{Au-Au} and N_{Au-Rh} should be

DOI: 10.1021/acs.langmuir.7b02857
Langmuir 2017, 33, 12434−12442

equal to the ratio of Au and Rh atoms, adjusted to account for the atomic fractions of the two metals in the NPs (eq 6).[36]

$$\frac{N_{Au-Au}}{N_{Au-Rh}} = \frac{n_{Au}}{n_{Rh}(1-x)} \quad (6)$$

For all of the RhAu DENs, however, the ratios of N_{Au-Au} and N_{Au-Rh} exceed the ratios of Au to Rh atoms present in the NPs by factors of ~2 to 5 (Table 4). This means that Au and Rh must be segregated, because the prevailing number of Au−Au bonds in the NPs shows that Au atoms prefer to form bonds with Au atoms over Rh atoms.[36] Note that similar conclusions may also be drawn from a comparison of the N_{Rh-Au} and N_{Rh-Rh} coordination numbers, but this information is not accessible for our samples as a result of the large uncertainties in the Rh coordination numbers.

Third, a comparison of N_{Rh} and N_{Au} provides insight into the location of segregated Rh and Au atoms, which could reside on the surface of the NPs or within their interior. For NPs with Rh segregated on the surface, one expects $N_{Rh} < N_{Au}$, whereas $N_{Rh} > N_{Au}$ suggests the segregation of Au to the surface.[36] In our case, N_{Rh} is significantly larger than N_{Au} for the G6-OH($Rh_{110}Au_{30}$) DENs (11 vs 7, Table 4); therefore, Au is segregated to the DEN surface. For NPs having lower Rh concentrations (G6-OH($Rh_{70}Au_{70}$) and G6-OH($Rh_{30}Au_{110}$) DENs), the uncertainties in N_{Rh} are too large to draw definitive conclusions about a particular segregation motif. Note, however, that the Au EXAFS analysis clearly indicates that segregation does occur.

Segregation of Rh and Au on either the surface or within the NPs is not surprising, because Rh and Au are immiscible in bulk materials, and hence RhAu alloys are expected to be thermodynamically unstable as a result of the higher cohesive and surface energies of Rh.[39] Theoretical simulations for unsupported and supported RhAu clusters containing a few hundred atoms also suggest the segregation of Rh and Au metals and, in particular, the segregation of Au to the NP surface. Surface segregation of Au in RhAu NPs has also previously been confirmed experimentally for titania-supported RhAu NPs.[40,41] These previous results are in agreement with our finding for Rh-rich RhAu DENs: Au atoms are segregated to the surface.[41] This suggests that there is no special thermodynamic driving force for atomic mixing in unsupported RhAu NPs, even in the case of NPs having the majority of their atoms residing on the surface (as is the case here).

SUMMARY AND CONCLUSIONS

In this study, we carried out in situ and ex situ XAS studies of Rh and RhAu DENs. The results show that under the conditions used in our study only a fraction of the Rh^{3+}-containing DEN precursors are fully reduced by $NaBH_4$. Moreover, by combining XAS and TEM data, we were able to demonstrate that fully reduced metallic particles coexist with unreduced Rh^{3+} species in both Rh and RhAu DENs. Because samples prepared in situ and ex situ exhibited similar structures, we concluded that air oxidation is slow compared to the XAS data acquisition time (~1 h). Accordingly, our results contradict those of Somorjai and co-workers.[13] We must point out, however, that there are some differences in experimental procedures. Specifically, the Somorjai group used G4-OH dendrimers and 40 equiv of Rh^{3+}, whereas here we used G6-OH and 140 equiv of Rh^{3+}. In addition, they used a 20-fold excess (with respect to Rh^{3+}) of $NaBH_4$, whereas we used a 10-fold excess to be consistent with most of the published literature. It seems unlikely that these slight procedural differences would affect the extent of Rh^{3+} reduction, but it is a possibility that should not be discounted.

Further structural analysis of RhAu alloy DENs using EXAFS leads to an alloy model in which Rh and Au are segregated. Moreover, in Rh-rich alloy DENs, Au atoms are specifically segregated to the surface. These findings are in agreement with the known immiscibility of Rh and Au in bulk alloys as well as with the previously reported theoretical simulations.[1]

ASSOCIATED CONTENT

Supporting Information

The Supporting Information is available free of charge on the ACS Publications website at DOI: 10.1021/acs.langmuir.7b02857.

Photographs of the solution cell used for the in situ EXAFS experiments; XANES data for Rh foil, Rh_2O_3, and RhAu alloy DENs at the Rh K-edge; XANES LCA fits for RhAu alloy DENs; XANES data for Au foil and RhAu alloy DENs at the Au L_3-edge; structural parameters obtained by fitting the EXAFS data of the RhAu alloy DENs; and STEM images of RhAu alloy DENs (PDF)

AUTHOR INFORMATION

Corresponding Authors

*E-mail: anatoly.frenkel@stonybrook.edu.
*E-mail: crooks@cm.utexas.edu.

ORCID

Long Luo: 0000-0001-5771-6892
Anatoly I. Frenkel: 0000-0002-5451-1207
Richard M. Crooks: 0000-0001-5186-4878

Present Address

‡Long Luo, Department of Chemistry, Wayne State University, 5101 Cass Avenue, Detroit, Michigan 48202, United States.

Author Contributions

∥These authors contributed equally.

Notes

The authors declare no competing financial interest.

ACKNOWLEDGMENTS

The authors gratefully acknowledge support from the U.S. National Science Foundation under the DMREF program (L.L., A.S.L., and R.M.C.: grant no. 1534177. A.I.F. and J.T.: grant no. 1726321). L.L., A.S.L., and R.M.C. also thank the Robert A. Welch Foundation (grant F-0032) for sustained research support. We also acknowledge the support of the BL2-2 beamline of the SSRL through the Synchrotron Catalysis Consortium (U.S. Department of Energy, Office of Basic Energy Sciences, grant no. DE-SC0012335). Finally, we thank Mr. Nicholas Marcella and Mr. Jiahao Huang from Stony Brook University for the help with the in situ EXAFS experiments.

REFERENCES

(1) García, S.; Zhang, L.; Piburn, G. W.; Henkelman, G.; Humphrey, S. M. Microwave Synthesis of Classically Immiscible Rhodium−Silver and Rhodium−Gold Alloy Nanoparticles: Highly Active Hydrogenation Catalysts. *ACS Nano* **2014**, *8*, 11512−11521.

(2) Fonseca, G. S.; Umpierre, A. P.; Fichtner, P. F.; Teixeira, S. R.; Dupont, J. The Use of Imidazolium Ionic Liquids for the Formation

DOI: 10.1021/acs.langmuir.7b02857
Langmuir 2017, 33, 12434−12442

and Stabilization of Ir0 and Rh0 Nanoparticles: Efficient Catalysts for the Hydrogenation of Arenes. *Chem. - Eur. J.* **2003**, *9*, 3263−3269.
(3) Jacinto, M. J.; Kiyohara, P. K.; Masunaga, S. H.; Jardim, R. F.; Rossi, L. M. Recoverable Rhodium Nanoparticles: Synthesis, Characterization and Catalytic Performance in Hydrogenation Reactions. *Appl. Catal., A* **2008**, *338*, 52−57.
(4) Yuan, Y.; Yan, N.; Dyson, P. J. Advances in the Rational Design of Rhodium Nanoparticle Catalysts: Control Via Manipulation of the Nanoparticle Core and Stabilizer. *ACS Catal.* **2012**, *2*, 1057−1069.
(5) Alayoglu, S.; Eichhorn, B. Rh−Pt Bimetallic Catalysts: Synthesis, Characterization, and Catalysis of Core−Shell, Alloy, and Monometallic Nanoparticles. *J. Am. Chem. Soc.* **2008**, *130*, 17479−17486.
(6) Park, J. Y.; Zhang, Y.; Grass, M.; Zhang, T.; Somorjai, G. A. Tuning of Catalytic Co Oxidation by Changing Composition of Rh-Pt Bimetallic Nanoparticles. *Nano Lett.* **2008**, *8*, 673−677.
(7) Renzas, J. R.; Huang, W.; Zhang, Y.; Grass, M. E.; Somorjai, G. A. Rh1−X Pd X Nanoparticle Composition Dependence in Co Oxidation by No. *Catal. Lett.* **2011**, *141*, 235−241.
(8) Anderson, R. M.; Yancey, D. F.; Zhang, L.; Chill, S. T.; Henkelman, G.; Crooks, R. M. A Theoretical and Experimental Approach for Correlating Nanoparticle Structure and Electrocatalytic Activity. *Acc. Chem. Res.* **2015**, *48*, 1351−1357.
(9) Myers, V. S.; Weir, M. G.; Carino, E. V.; Yancey, D. F.; Pande, S.; Crooks, R. M. Dendrimer-Encapsulated Nanoparticles: New Synthetic and Characterization Methods and Catalytic Applications. *Chem. Sci.* **2011**, *2*, 1632−1646.
(10) Chung, Y.-M.; Rhee, H.-K. Partial Hydrogenation of 1,3-Cyclooctadiene Using Dendrimer-Encapsulated Pd−Rh Bimetallic Nanoparticles. *J. Mol. Catal. A: Chem.* **2003**, *206*, 291−298.
(11) Peng, X.; Pan, Q.; Rempel, G. L. Bimetallic Dendrimer-Encapsulated Nanoparticles as Catalysts: A Review of the Research Advances. *Chem. Soc. Rev.* **2008**, *37*, 1619−1628.
(12) Huang, W.; Kuhn, J. N.; Tsung, C.-K.; Zhang, Y.; Habas, S. E.; Yang, P.; Somorjai, G. A. Dendrimer Templated Synthesis of One Nanometer Rh and Pt Particles Supported on Mesoporous Silica: Catalytic Activity for Ethylene and Pyrrole Hydrogenation. *Nano Lett.* **2008**, *8*, 2027−2034.
(13) Borodko, Y.; Thompson, C. M.; Huang, W.; Yildiz, H. B.; Frei, H.; Somorjai, G. A. Spectroscopic Study of Platinum and Rhodium Dendrimer (Pamam G4oh) Compounds: Structure and Stability. *J. Phys. Chem. C* **2011**, *115*, 4757−4767.
(14) Deraedt, C.; Melaet, G.; Ralston, W. T.; Ye, R.; Somorjai, G. A. Platinum and Other Transition Metal Nanoclusters (Pd, Rh) Stabilized by Pamam Dendrimer as Excellent Heterogeneous Catalysts: Application to the Methylcyclopentane (Mcp) Hydrogenative Isomerization. *Nano Lett.* **2017**, *17*, 1853−1862.
(15) Ye, R.; Yuan, B.; Zhao, J.; Ralston, W. T.; Wu, C.-Y.; Unel Barin, E.; Toste, F. D.; Somorjai, G. A. Metal Nanoparticles Catalyzed Selective Carbon−Carbon Bond Activation in the Liquid Phase. *J. Am. Chem. Soc.* **2016**, *138*, 8533−8537.
(16) Siani, A.; Alexeev, O. S.; Samuel Deutsch, D.; Monnier, J. R.; Fanson, P. T.; Hirata, H.; Matsumoto, S.; Williams, C. T.; Amiridis, M. D. Dendrimer-Mediated Synthesis of Subnanometer-Sized Rh Particles Supported on Zro2. *J. Catal.* **2009**, *266*, 331−342.
(17) Newville, M. Ifeffit: Interactive Xafs Analysis and Feff Fitting. *J. Synchrotron Radiat.* **2001**, *8*, 322−324.
(18) Ravel, B.; Newville, M. Athena, Artemis, Hephaestus: Data Analysis for X-Ray Absorption Spectroscopy Using Ifeffit. *J. Synchrotron Radiat.* **2005**, *12*, 537−541.
(19) Scott, R. W.; Ye, H.; Henriquez, R. R.; Crooks, R. M. Synthesis, Characterization, and Stability of Dendrimer-Encapsulated Palladium Nanoparticles. *Chem. Mater.* **2003**, *15*, 3873−3878.
(20) Anderson, R. M.; Yancey, D. F.; Loussaert, J. A.; Crooks, R. M. Multistep Galvanic Exchange Synthesis Yielding Fully Reduced Pt Dendrimer-Encapsulated Nanoparticles. *Langmuir* **2014**, *30*, 15009−15015.
(21) Anderson, R. M.; Zhang, L.; Loussaert, J. A.; Frenkel, A. I.; Henkelman, G.; Crooks, R. M. An Experimental and Theoretical Investigation of the Inversion of Pd@Pt Core@Shell Dendrimer-Encapsulated Nanoparticles. *ACS Nano* **2013**, *7*, 9345−9353.
(22) Alvarez, M. M.; Khoury, J. T.; Schaaff, T. G.; Shafigullin, M. N.; Vezmar, I.; Whetten, R. L. Optical Absorption Spectra of Nanocrystal Gold Molecules. *J. Phys. Chem. B* **1997**, *101*, 3706−3712.
(23) Luo, L.; Zhang, L.; Henkelman, G.; Crooks, R. M. Unusual Activity Trend for Co Oxidation on Pdxau140−X@Pt Core@Shell Nanoparticle Electrocatalysts. *J. Phys. Chem. Lett.* **2015**, *6*, 2562−2568.
(24) Luo, L.; Zhang, L.; Duan, Z.; Lapp, A. S.; Henkelman, G.; Crooks, R. M. Efficient Co Oxidation Using Dendrimer-Encapsulated Pt Nanoparticles Activated with < 2% Cu Surface Atoms. *ACS Nano* **2016**, *10*, 8760−8769.
(25) Luo, L.; Duan, Z.; Li, H.; Kim, J.; Henkelman, G.; Crooks, R. M. Tunability of the Adsorbate Binding on Bimetallic Alloy Nanoparticles for the Optimization of Catalytic Hydrogenation. *J. Am. Chem. Soc.* **2017**, *139*, 5538.
(26) Knecht, M. R.; Weir, M. G.; Myers, V. S.; Pyrz, W. D.; Ye, H.; Petkov, V.; Buttrey, D. J.; Frenkel, A. I.; Crooks, R. M. Synthesis and Characterization of Pt Dendrimer-Encapsulated Nanoparticles: Effect of the Template on Nanoparticle Formation. *Chem. Mater.* **2008**, *20*, 5218−5228.
(27) Bunker, G. *Introduction to XAFS: A Practical Guide to X-ray Absorption Fine Structure Spectroscopy*; Cambridge University Press, 2010.
(28) Koningsberger, D.; Prins, R. X-ray Absorption: Principles, Applications, Techniques of EXAFS, SEXAFS, and XANES. 1988.
(29) Benfatto, M.; Meneghini, C. A Close Look into the Low Energy Region of the XAS Spectra: The XANES Region. In *Synchrotron Radiation: Basics, Methods and Applications*; Mobilio, S., Boscherini, F., Meneghini, C., Eds.; Springer: Berlin, 2015; pp 213−240.
(30) Kuzmin, A.; Chaboy, J.; Exafs. EXAFS and XANES Analysis of Oxides at the Nanoscale. *IUCrJ* **2014**, *1*, 571−589.
(31) Lei, Y.; Jelic, J.; Nitsche, L. C.; Meyer, R.; Miller, J. Effect of Particle Size and Adsorbates on the L3, L2 and L1 X-Ray Absorption near Edge Structure of Supported Pt Nanoparticles. *Top. Catal.* **2011**, *54*, 334−348.
(32) Ankudinov, A.; Rehr, J.; Low, J. J.; Bare, S. R. Sensitivity of Pt X-Ray Absorption near Edge Structure to the Morphology of Small Pt Clusters. *J. Chem. Phys.* **2002**, *116*, 1911−1919.
(33) Timoshenko, J.; Shivhare, A.; Scott, R. W.; Lu, D.; Frenkel, A. I. Solving Local Structure around Dopants in Metal Nanoparticles with Ab Initio Modeling of X-Ray Absorption near Edge Structure. *Phys. Chem. Chem. Phys.* **2016**, *18*, 19621−19630.
(34) Newville, M.; Ravel, B.; Haskel, D.; Rehr, J.; Stern, E.; Yacoby, Y. Analysis of Multiple-Scattering Xafs Data Using Theoretical Standards. *Phys. B* **1995**, *208-209*, 154−156.
(35) Ankudinov, A.; Ravel, B.; Rehr, J.; Conradson, S. Real-Space Multiple-Scattering Calculation and Interpretation of X-Ray-Absorption near-Edge Structure. *Phys. Rev. B: Condens. Matter Mater. Phys.* **1998**, *58*, 7565.
(36) Frenkel, A. I. Applications of Extended X-Ray Absorption Fine-Structure Spectroscopy to Studies of Bimetallic Nanoparticle Catalysts. *Chem. Soc. Rev.* **2012**, *41*, 8163−8178.
(37) Zhang, H.; Deng, X.; Jiao, C.; Lu, L.; Zhang, S. Preparation and Catalytic Activities for H2o2 Decomposition of Rh/Au Bimetallic Nanoparticles. *Mater. Res. Bull.* **2016**, *79*, 29−35.
(38) Ovári, L.; Bugyi, L.; Majzik, Z.; Berkó, A.; Kiss, J. Surface Structure and Composition of Au− Rh Bimetallic Nanoclusters on Tio2 (110): A Leis and Stm Study. *J. Phys. Chem. C* **2008**, *112*, 18011−18016.
(39) Konuspayeva, Z.; Afanasiev, P.; Nguyen, T.-S.; Di Felice, L.; Morfin, F.; Nguyen, N.-T.; Nelayah, J.; Ricolleau, C.; Li, Z.; Yuan, J. Au−Rh and Au−Pd Nanocatalysts Supported on Rutile Titania Nanorods: Structure and Chemical Stability. *Phys. Chem. Chem. Phys.* **2015**, *17*, 28112−28120.
(40) Ovári, L.; Bugyi, L.; Majzik, Z.; Berkó, A.; Kiss, J. Surface Structure and Composition of Au-Rh Bimetallic Nanoclusters on Tio2 (110): A Leis and Stm Study. *J. Phys. Chem. C* **2008**, *112*, 18011−18016.

DOI: 10.1021/acs.langmuir.7b02857
Langmuir 2017, 33, 12434−12442

(41) Piccolo, L.; Li, Z.; Demiroglu, I.; Moyon, F.; Konuspayeva, Z.; Berhault, G.; Afanasiev, P.; Lefebvre, W.; Yuan, J.; Johnston, R. L. Understanding and Controlling the Structure and Segregation Behaviour of Aurh Nanocatalysts. *Sci. Rep.* **2016**, *6*, 6.

DOI: 10.1021/acs.langmuir.7b02857
Langmuir 2017, 33, 12434−12442